UHF FILM RESONATOR EVALUATION AND RESONATOR-CONTROLLED OSCILLATOR AND FILTER DESIGN USING COMPUTER-AIDED DESIGN TECHNIQUES

M.M. Driscoll,* S.V. Krishnaswamy,+ R.A. Moore,* and J.R. Szedon+

* Westinghouse Defense and Electronics Center, Baltimore, MD 21203
+ Westinghouse Research and Development Center, Pittsburgh, PA 15235

ABSTRACT

RF magnetron-sputtered piezoelectric films on silicon semiconductor substrates provide the basis for high Q, temperature-stable, bulk acoustic resonators in monolithic, UHF signal processing circuits. This paper describes the design of UHF oscillators using such resonators as the frequency-controlling elements. RF circuit analysis/optimization software has been used for determining resonator equivalent electrical circuit parameters and oscillator sustaining-stage optimum small-signal impedance characteristics, based on automated measurement of resonator and transistor S-parameters. Oscillator circuits have been designed for potential implementation using silicon and GaAs technology. A prototype oscillator has been fabricated that is realizable in monolithic form and allows resonator utilization as a one port. Measurement of oscillator output-signal phase-noise sideband spectra indicates achievement of L(f) = −110 dB/Hz at 1 kHz carrier offset frequency.

INTRODUCTION

During recent years, work has been progressing toward the development of a reproducible deposition process for fabrication of extremely small volume, UHF, piezoelectric resonators on semiconductor substrates under conditions compatible with the processing of active devices on the same substrate [1-6]. The goal of these efforts is the development of a wide variety of UHF signal processing circuits, including the requisite frequency-selective components, in fully monolithic form.

Film bulk acoustic resonators (FBARs) have been fabricated by magnetron sputtering of thin films of piezoelectric material such as aluminum nitride and zinc oxide onto silicon and gallium arsenide substrates [4-8].

The electrical equivalent circuit of the FBAR that describes the device desired resonance and nonresonant electrical impedance is similar to that of conventional bulk wave quartz crystal resonators. Because the FBAR operates over the UHF band, however, the resonator test enclosure and enclosure connection impedances tend to mask the actual FBAR impedance characteristic to a greater degree than in the case of VHF quartz resonators. A measurement technique that provides accurate determination of FBAR equivalent circuit element values is a requirement for evaluation and optimization of resonator processing methods. FBAR equivalent circuit data is also useful for the design and analysis of more complex circuitry incorporating the resonators as circuit components.

This paper describes the use of Super Compact® RF circuit analysis/optimization software, in conjunction with automatic network analyzer measurement of resonator and active device small-signal scattering parameters, for the purpose of FBAR evaluation/equivalent circuit modeling and FBAR-stabilized oscillator design.* The techniques described in this paper are readily applicable to the use of other RF circuit analysis/optimization software as well.

*Super Compact is a registered trademark of Compact Software, Inc, a COMSAT company.

RESONATOR MODELING PROCEDURE

The dashed curve of figure 1 shows a Smith chart plot of the impedance characteristic of a composite (aluminum nitride on silicon) resonator fabricated at Westinghouse. As shown in the figure, the plotted data may be grouped into a near-resonance region, designated by points C through F, and off-resonance regions, designated by points A, B, G, and H. In actual practice, the measured data is recorded as a listing of small-signal scattering parameters (S_{11}). Since the resonators are packaged in sealed TO-5 enclosures, the measurement procedure includes software-controlled calibration of the network analyzer and associated TO-5 test fixture. Shorted and open-pin TO-5 headers were used for separate determination of header pin inductance and pin-to-header-base capacitance.

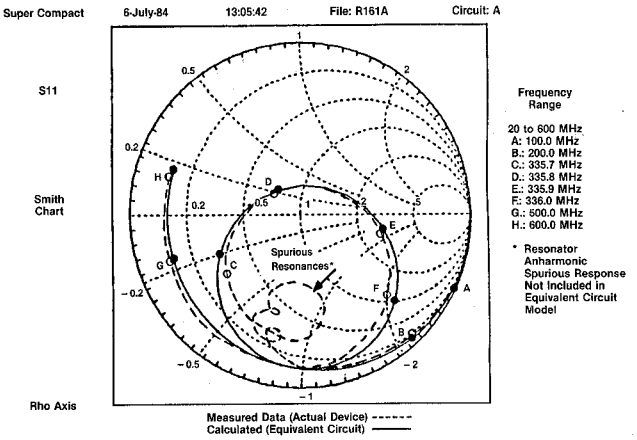

Figure 1. Comparison of Resonator Impedance for Actual Device and Equivalent Circuit Model

The measured data is entered in a circuit file to be used in conjunction with the circuit analysis/optimization software for determining resonator wire-bond impedance and static capacitance and calculating resonator motional branch impedance. Figure 2 shows the schematic diagram for the resonator as entered in the software circuit file. The software, through a random optimization routine, establishes the (negative) values for bond-wire impedance and resonator static capacitance such that extraction of these values (and those of the package parasitic reactances) from the measured resonator S_{11} data yields a high impedance value at off-resonance frequencies. The residual impedance (representing that of the resonator motional branch) is calculated and printed as output data, as shown in figure 3. The resonator motional branch element values are easily calculated from the output data, and

0149-645X/85/0000−0239 $01.00 © 1985 IEEE

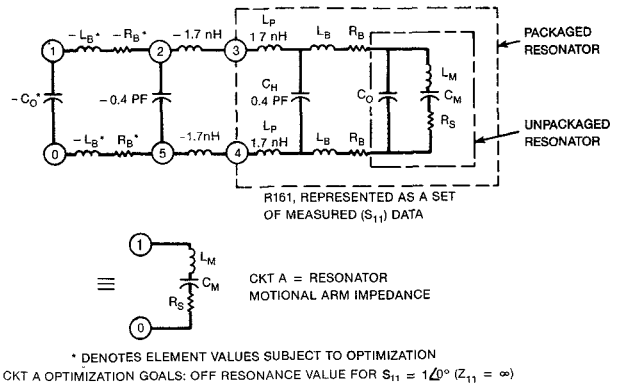

Figure 2. Resonator Schematic Diagram as Utilized in Software Analysis Circuit File

CIRCUIT: A — IMPEDANCE (ohms)

FREQ (MHz)	RESISTANCE	REACTANCE
100.00000	−4086.071	−4926.671
200.00000	−2531.280	−456.345
300.00000	−2356.094	698.015
335.70001	44.463	−74.546
335.75003	42.563	−33.017
335.79999	39.427	0.085
335.85001	40.638	32.131
335.89999	41.608	63.779
335.95001	40.703	95.433
336.00000	41.919	124.597
400.00000	−826.839	2156.124
500.00000	870.131	6164.011
600.00000	−3301.758	−1153.023

FROM CALCULATED CIRCUIT A (RESONATOR MOTIONAL) IMPEDANCE:

$R_S \simeq 40$ ohms

$F_S \simeq 335.800$MHz

$$L_M \simeq \frac{1}{4\pi}\frac{\Delta X}{\Delta F} \simeq \frac{1}{4\pi}\frac{32 \text{ ohms}}{5 \times 10^4 \text{ Hz}} \simeq 51\ \mu H$$

$$\therefore C_M \simeq .004405 \text{ pF}$$

FINAL (SOFTWARE OPTIMIZED) ELEMENT VALUES:

$C_O = 6.14$ pF $L_B = 5.15$ nH $R_B = 3.15$ ohms

$\therefore C_O/C_M = 1400$ $\therefore Q_M = \frac{2\pi F_S L_M}{R_S} \simeq 2690$

Figure 3. Software Analysis Results and Associated Calculation of Resonator Motional Element Values and Resonant Frequency

the optimized (best-fit) values for resonator static capacitance and wire-bond impedance are automatically entered into the circuit file.

Use of this modeling procedure has been found to yield results such that excellent agreement exists between actual device measured data and calculated equivalent-circuit model impedance, as shown in figure 1.

Table 1 summarizes some of the modeling results for AlN film resonators that were sputter-deposited under different gas compositions.

Table 1. Film Resonator Modeling Results With Fabrication Details

Sample No.	C_o (pF)	L (μH)	RS (Ω)	Q_m	C_o/C_m	F_S (MHz)	Membrane Dimension (μm)	Top Electrode Dimension (μm)	Membrane Thickness (μm)	AlN Thickness (μm)	Argon Partial Pressure* (mTorr)
R-123	3.47	220	78	9000	7800	510.000	650	250	7	1.64	0.0
R-159	3.22	100	110	2900	3200	503.569	650	250	7	1.6	0.5
R-161	6.19	72	35	4300	1990	335.825	1200	500	7	3.7	1.0
R-170	3.98	82.5	45	4580	2060	397.48	650	250	3	3.4	1.0
R-172	1.47	160	90	4336	1400	388.20	350	150	3	3.4	1.0
R-218	2.66	57	50	2550	759	356.085	650	250	8.9	3.6	2.0

*Total Sputtering Pressure (Nitrogen and Argon): 4.0 mTorr

We chose as the baseline device one of the resonators (R-123) for which the AlN film was deposited in pure nitrogen. This resonator exhibited a very high unloaded (motional branch) Q; however, the C_o/C_m ratio, whose reciprocal is proportional to the square of the electromechanical coupling coefficient (k^2), was high. As seen from the table, addition of argon to the sputtering gas appears to improve (lower) the capacitance ratio.

FILM RESONATOR CONTROLLED OSCILLATOR

Several factors were considered in a design of the 336 MHz FBAR-stabilized oscillator sustaining-stage circuit. It was desirable that the circuit be inductorless to ensure eventually the simplest implementation in monolithic form on a semiconductor substrate. In this regard, an additional circuit design goal was to have the resonator connected with the bottom electrode at ground. It was also decided initially to use silicon bipolar transistors since FBAR processing on silicon was more advanced than that on GaAs.

A two-transistor, Pierce type oscillator arrangement was considered, as shown in figure 4. When the resonator bottom electrode is connected to ground, it is convenient to view the sustaining circuit as a negative resistance generator.

In the oscillator circuit of figure 4, steady state conditions are achieved when the resonator impedance and that of the sustaining stage are equal in magnitude and opposite in sign. Oscillator operation normally occurs at a frequency slightly above resonator series resonance where the resonator inductive reactance is equal in magnitude to the reactance of C_1 in series with C_2, and where the negative resistive portion of the sustaining stage impedance is equal to the positive resistance of the resonator impedance.

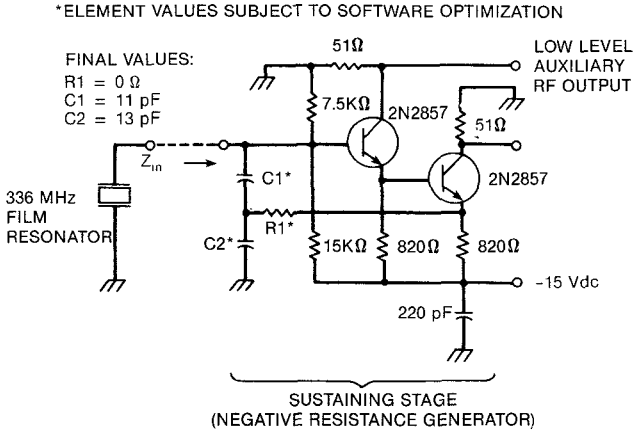

SOFTWARE OPTIMIZATION GOALS:

$F \leq 235$ MHz $IM(Z_{in}) \leq 0$

$F = 335$ MHz $Z_{in} = -34 + j9$

$F \geq 535$ MHz $R_E(Z_{in}) \geq 0$

OPTIMIZATION RESULTS:

FREQ (GHz)	IMPEDANCE (ohms) RESISTANCE	REACTANCE
0.13500	−382.091	−781.117
0.23500	−199.907	−0.332
0.33500	−34.302	8.790
0.43500	−5.082	−6.118
0.53500	2.677	−12.808
0.63500	4.703	−14.976
0.73500	5.231	−15.640
0.83500	5.394	−15.770
0.93500	5.380	−15.790
1.03500	5.396	−15.700

Figure 4. FBAR Oscillator Circuit and Circuit Analysis Results

Oscillator circuit small-signal excess gain is required in order that oscillation is initiated upon application of dc power to the circuit, and is provided by selecting R_1, C_1, and C_2 such that the negative resistive portion of the sustaining-stage impedance is typically 1.5 to 2 times larger than the resistive portion of the resonator impedance. Steady-state conditions are reached by providing a mechanism for reducing

effective transconductance (g_m) with increasing signal level. This is commonly achieved by simply letting the transistor of figure 4 current-limit.

Referring again to figure 1, note that the most desirable oscillator operating frequency is in the vicinity of point C, where the resonator impedance phase slope is a maximum. At this frequency, the resonator impedance is approximately 17 − j9 ohms. Oscillator excess gain requirements dictate that the sustaining stage impedance exhibit an equal and opposite reactive value and a negative resistance value approximately twice that of the resonator, or −34 + j9 ohms.

As stated previously, the Pierce sustaining-stage impedance at the resonator connection terminals normally exhibits a capacitive reactance, and oscillator operation at point C of figure 1 would not be possible. However, in UHF oscillators employing transistors operating at 20 to 50 percent of their gain-bandwidth products, the effects of transistor interterminal reactance and resistance (and propagation delay) become nonnegligible. It has been found that the two-stage circuit of figure 4, as a result of these effects, can be made to exhibit a negative resistive input impedance whose reactive component is predictably inductive.

The method used in the design of the oscillator sustaining stage may be summarized as follows:

1. Selection of transistor and transistor dc operating point
2. Measurement of transistor (common collector) small-signal S-parameters
3. Sustaining-stage circuit simulation/optimization using Super Compact analysis software

Step 3 involves automatic software optimization of sustaining-stage capacitor and unbypassed emitter resistor values to achieve the desired small-signal input impedance characteristics required for oscillation at the desired (resonator impedance) operating point while preventing potential oscillation at out-of-band frequencies.

Figure 4 shows the results of the software circuit analysis/optimization computations. The figure 4 circuit was fabricated using discrete chip components. Oscillator operation without tuning was within 50 kHz of the desired (predicted) operating frequency. The results of oscillator signal phase-noise sideband spectral measurements are shown in figure 5. Phase noise measurements were also made for the case of a one-port 320 MHz SAW resonator substituted for the FBAR. The results are important because they show achievement of comparable performance when differences in resonator Q are taken into account.

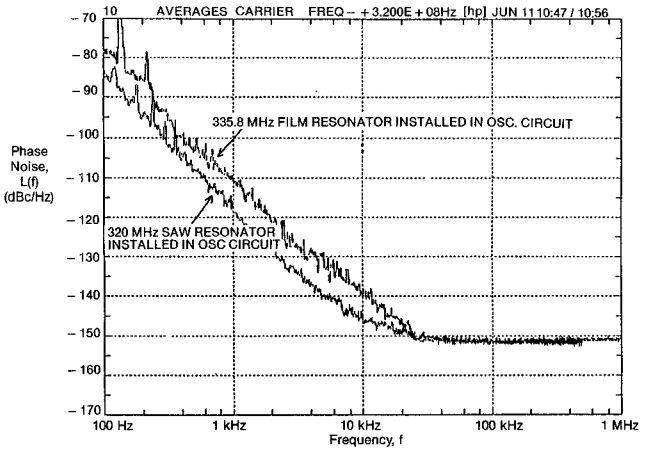

Figure 5. Comparison of Oscillator Phase Noise Using Surface Wave and Bulk Wave Film Resonators

With regard to film resonator circuit applications, recent emphasis has been placed on using circuits employing GaAs active devices. Although resonators were originally processed on silicon, it has been recognized that resonator use will be at UHF (300-3000 MHz), and active device and eventual resonator fabrication on GaAs will be required for monolithic circuits capable of operation over this frequency range. We have shown that the extremely low parasitic reactance and resulting small propagation delay associated with GaAs active devices can be utilized to design film resonator filter and oscillator circuitry not implementable using silicon based technology. For example, figure 6(a) shows the conventional method of resonator static capacitance neutralization in single and multipole VHF quartz crystal filters using balanced transformers. Figure 6(b) shows how a pair of gain-matched inverting and noninverting amplifiers can be used to approximate, in monolithic form, resonator capacitance neutralization. Low propagation delay GaAs FET amplifiers are ideally suited to this application.

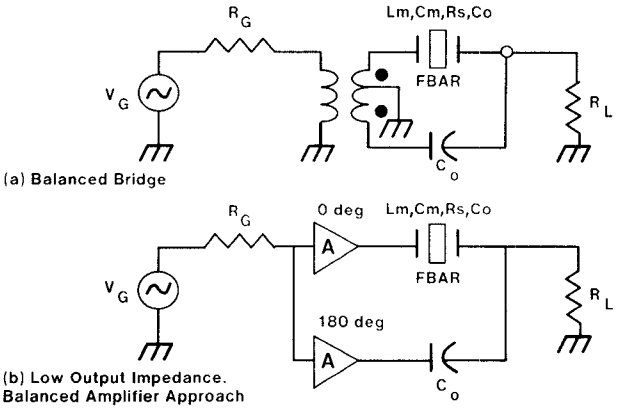

Figure 6. MMIC Circuit Approach for Neutralization of FBAR Static Capacitance

Figure 7 shows the actual measured results of a simple breadboard neutralization circuit incorporating three S-band GaAs FETs. Without any attempt at trimming, 14-dB filter stopband attenuation has been achieved on a per-pole (single resonator) basis. This implies that four such cascaded sections would exhibit quite respectable (56 dB) stopband performance.

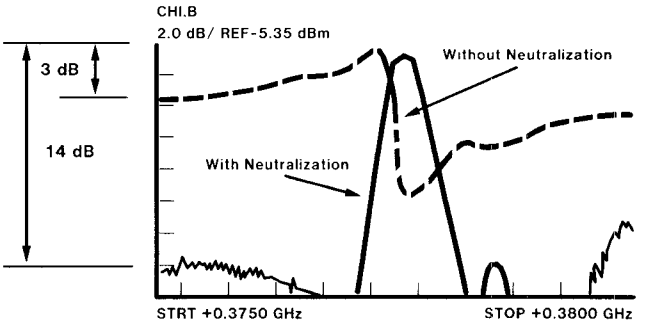

Figure 7. Active Circuit Neutralization of FBAR Static Capacitance Using GaAs Transistors

Film resonator oscillator circuitry using GaAs active circuitry has also been designed. Figure 8 shows a candidate dual-transistor Butler oscillator configuration. The advantages of the Butler configuration are:

1. Pure negative resistance is generated at the resonator terminals, allowing oscillator operation at series resonance where maximum tuning range and highest resonator unloaded-Q are obtainable.
2. Negative resistance is generated over only a confined, designed bandwidth, allowing resonator operation at a harmonic resonance while eliminating the possibility of instability at undesired FBAR resonant frequencies.
3. Tuned circuit Q is low, allowing use of noncritical tank circuit elements, including low inductance easily implementable in monolithic form.
4. The sustaining stage can be configured to allow placement of the

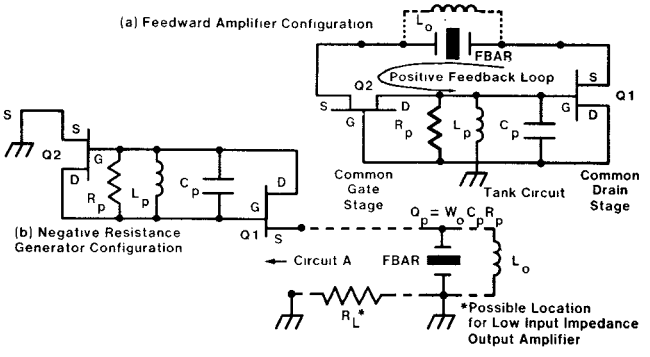

Figure 8. Functional Schematic Diagram for Two-Transistor FBAR Butler Oscillator

resonator in series with the buffer amplifier load circuitry. Thus, the narrow-band frequency selectivity of the resonator impedance characteristic can act to filter the oscillator output-signal noise spectra. In instances where it is advantageous to connect the resonator bottom electrode to ground, the same configuration may be utilized, except that the buffer amplifier input signal is extracted from a different portion of the sustaining stage circuitry.

Figure 9 shows the results of Super Compact analysis/optimization of the figure 8 circuit, based on measured GaAs FET small-signal scattering parameters.

Optimization Goal
Circuit A Input Impedance
at F_o = 1200 MHz = −50 + j0

Results: C_p = 4.4 pF, L_p = 3.6 nH, Q_p = 4
Circuit: A

	Impedance (Ohms)	
Freq (GHz)	Resistance	Reactance
0.600	36.364	−14.388
0.700	33.924	−18.377
0.800	29.820	−23.187
0.900	22.580	−28.864
1.000	8.971	−34.483
1.100	−17.163	−33.476
1.200	−50.006	−0.008
1.300	−29.610	55.846
1.400	12.795	61.586
1.500	32.823	49.102
1.600	40.913	37.979
1.700	44.429	29.758
1.800	46.045	23.651

Figure 9. Small-Signal Computer Analysis and Optimization Results for the Butler Oscillator Sustaining Stage

CONCLUSIONS

An automated UHF resonator measurement and accurate modeling procedure has been developed using computer-controlled hardware and circuit analysis software. This approach indicates that improved electromechanical coupling can be achieved in AlN films by reactive RF magnetron sputtering in a 1:1 mixture of argon and nitrogen.

This procedure will be an important aid in evaluation and refinement of resonator fabrication procedures, and that is useful in the design and analysis of more complex circuits containing FBARs as circuit components.

The amenability of FBAR circuitry to CAD circuit simulation has been demonstrated.

RF analysis/optimization software has been successfully utilized in the development of oscillator and filter circuitry employing the FBAR as the frequency-controlling element. The circuits can be implemented in monolithic form and allow utilization of composite resonators exhibiting high capacitance ratio. Measurement of prototype oscillator short-term stability indicates that established relationships between sustaining-stage active-device noise spectra and oscillator closed-loop signal stability are valid for the FBAR oscillator.

REFERENCES

[1] K.M. Lakin and J.S. Wang, *Proc. 1980 Ultrasonics Symp.* (IEEE, New York, 1980), p. 83.
[2] T.W. Greudkowski, J.F. Black, T.M. Reeder, D.E. Cullen, and R.A. Wagner, *Appl, Phys. Lett.*, 37 (1980), 993.
[3] T. Shiosaki, T. Yamamoto, T. Oda, and A. Kawabata, *Appl. Phys. Lett.*, 36 (1980), 643.
[4] K.M. Lakin and J.S. Wang, *Appl. Phys. Lett.*, 38 (1981), 125.
[5] J.S. Wang and K.M. Lakin, *Appl. Phys. Lett.*, 40 (1982), 308.
[6] K.M. Lakin, J.S. Wang and A.R. Landin, *Proc. 36th Freq. Control Symp.* (1982), p. 346.
[7] G.R. Kline and K.M. Lakin, *Proc. 1983 Ultrasonics Symp.* (IEEE, New York, 1983), p. 495.
[8] K. Tsubouchi and N. Mikoshiba, *Proc. 1983 Ultrasonics Symp.* (IEEE, New York, 1983), p. 299.
[9] S.G. Burns and R.S. Ketcham, *1984 MTT-S Symp. Digest* (IEEE, New York, 1984), p. 83.
[10] S.V. Krishnaswamy, W.A. Hester, J.R. Szedon, M.M. Driscoll, and M.H. Francombe, to be published in *Thin Solid Films.*